

MIT Open Access Articles

Selective Sulfidation for Rare Earth Element Separation

The MIT Faculty has made this article openly available. **Please share** how this access benefits you. Your story matters.

Citation: Stinn, C., Allanore, A. (2022). Selective Sulfidation for Rare Earth Element Separation. In: Ouchi, T., et al. Rare Metal Technology 2022. The Minerals, Metals & Materials Series. Springer, Cham.

As Published: 10.1007/978-3-030-92662-5_25

Publisher: Springer International Publishing

Persistent URL: <https://hdl.handle.net/1721.1/153476>

Version: Author's final manuscript: final author's manuscript post peer review, without publisher's formatting or copy editing

Terms of use: Creative Commons Attribution-Noncommercial-Share Alike



Selective Sulfidation for Rare Earth Element Separation

Caspar Stinn¹ and Antoine Allanore^{1*}

Massachusetts Institute of Technology, Department of Materials Science and Engineering, 77 Massachusetts Avenue, Cambridge, MA 02139, USA

* Corresponding Author: allanore@mit.edu

Abstract

Rare earth metals and compounds are critical components of advanced materials for energy, structural alloys, and transportation. These low-tonnage elements are sourced together as by- and co-products, and presently require complete hydrometallurgical dissolution followed by liquid-liquid separation for their isolation and production. There is great interest in developing alternatives to those hydrometallurgical processes in order to limit the environmental impact of rare-earth element supply. Herein, we present selective sulfidation as a novel, high-temperature alternative to facilitate physical separation of rare earth by- and co-product elements. We explore the thermodynamics of rare earth oxide sulfidation with elemental sulfur, and discuss the role of carbon in controlling sulfidation selectivity. We apply these findings to the demonstration of selective sulfidation for iron-rare earth and lanthanide-lanthanide separations.

Keywords: Sulfidation, Rare-earth separation, Lanthanides, Scandium, Pyrometallurgy, Physical separation

Introduction

Rare earth elements are required for a broad range of technologies essential to modern society, ranging from neodymium and dysprosium for high-strength magnets to cerium for automotive catalytic converters to scandium for aerospace aluminum alloys[1]. These elements, consisting of the lanthanides, scandium, and yttrium, are found together in nature and are produced as co- and by-products of one another[2]. Despite being classified as “rare earth” elements, they are relatively common within the earth’s crust – on par with many base metals. For example, the crustal abundance of neodymium is on the same order of magnitude of nickel, zinc, and copper, twice that of cobalt, three times that of lead, and twenty times that of tin[3]. Nevertheless, commercially-viable deposits of rare earth elements are geographically concentrated, with China accounting for over 60% of recorded global production in 2020, followed by the United States at about 15%[4]. Concerns over supply stability, and the lack of suitable substitutes for rare earth elements in many applications, has led rare earth elements to be classified as critical and strategically-significant materials by numerous governments[5]. Challenges surrounding rare earth element supply are further compounded by the “balance problem”[6,7]. The “balance problem” refers to the reality that the distribution of demand between individual rare earth elements does not match up with their relative abundances in commercially-relevant mineral bodies. This disconnect between supply and demand results in production being driven by a few, high-demand elements such as neodymium, with oversaturated supplies of lower demand rare earth elements.

Rare earth elements may be grouped into two main categories: light (La, Ce, Pr, Nd, Pm, Sm) and heavy (Eu, Gd, Tb, Dy, Ho, Er, Tm, Yb, Lu, Sc, Y). Light rare earth elements are most commonly produced from the fluorocarbonate mineral bastnaesite and phosphate mineral monazite, whereas heavy rare earth elements are more concentrated in the phosphate mineral xenotime and in lateritic ion absorption clays[2]. No distinct mineral phases of individual lanthanide elements exist; they are all present, substituted for one another within the mineral. Actinides including thorium and uranium are also present as normally occurring radioactive materials (NORMs) in rare earth minerals through atomic substitution with the lanthanides[8]. Scandium meanwhile may also be found and produced as a byproduct of nickel production from lateritic ore deposits[9–11]. Furthermore, significant attention has been directed toward recovery of scandium from the red-mud tailings of the Bayer process for alumina production from bauxite[12–14], yet separating scandium from iron remains a difficult task[10].

Conventional rare earth element production from fluorocarbonate and phosphate mineral sources begins with mining, comminution, and physical separation to produce a rare earth mineral concentrate[15,16]. The rare earth concentrate is chemically digested, or “cracked”, via acid or alkaline treatment, with the rare earth elements leached into an aqueous solution for individual separation via aqueous-organic liquid-liquid solvent extraction. During the cracking and leaching process, the majority of NORMs and entrained transition and alkaline earth metal impurities remain with the leach residue or are selectively precipitated[2]. Due to the chemical similarity of rare earth elements, solvent extraction is a very energy and chemical intensive process, with individual rare earth separations each generally requiring on the order of 50 to 150 extraction and stripping stages for separation[2]. The separated rare earth element is then precipitated as a pure compound. The pure compound may then be calcined to form an oxide, halogenated, and/or reduced to metal via molten salt electrolysis or metallothermic reduction[17].

The environmental impact of rare earth metal reduction is greatly dependent on the process employed[18]. In the rare earth element separation pathway upstream of reduction, the environment impact is largely inherited from the solvent extraction steps[19]. For rare earth element separation from bastnaesite, solvent extraction contributes approximately 77% to the terrestrial acidification, 63% to the global warming potential, and 70% to the water usage of the entire rare earth element mining, beneficiation, and separation pathway[8]. Solvent extraction in monazite processing exhibits similar environmental burdens. When processing steps in the rare earth element mining, beneficiation, and separation pathway are normalized by material throughput, solvent extraction is likewise the largest contributor to process capital cost by an order of magnitude[20–23]. The economic and environmental impact of liquid-liquid processing motivates efforts to develop new methods of rare earth element separation with reduced environmental and capital footprints.

Numerous hydrometallurgical methods have been explored to improve the thermodynamics and sustainability of solvent extraction, ranging from new organic collector phases[24] to introducing magnetic fields during the hydrometallurgical process[25]. However, even highly-optimized solvent extraction systems for readily separated base metals, such as iron-copper or nickel-cobalt, still exhibit large energy and environmental impacts[26]. This suggests that incremental improvements to the hydrometallurgy of rare earth elements separation ultimately has limited promise in greatly reducing the overall environmental burden of rare earth element separation. In general, physical processes to separate elements isolated in distinct mineral phases exhibit lower environmental impacts than chemical processes to separate elements mixed in multi-element compounds or solid solutions[27,28]. Therefore, a low-cost, low-energy, and sustainable pretreatment to partition (“crack”) mixed rare earth element compounds to distinct, physically-separable phases of individual rare earth elements is an attractive method to reduce the energy and economic burden of rare earth element separation.

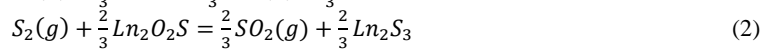
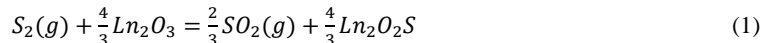
A variety of halide, sulfate, and borate-based pretreatments to partition rare earth elements from a multi-element compound feed into distinct phases for physical separation have been explored. Chemical vapor transportation has been studied to separate rare earth elements through differences in volatility and stoichiometry of their respective rare earth-aluminum chloride vapor complexes[29]. Meanwhile, reactive vacuum distillation has been explored for separation of divalent and trivalent rare-earth chlorides and iodides, also based on differences in volatility[30]. However, halogenation chemistry for metal compounds also exhibits significant environmental impacts and costs associate with toxic reagents such as chlorine, hydrogen fluoride, and phosgene gasses[31,32]. Selective acid roasting or sulfation with sulfur dioxide has been considered to promote selective leaching of rare earth elements[33–37], yet acid roasting processes too exhibit significant environmental impacts when applied to rare earth element processing[8]. Finally, while borate crystallization or slag refining shows good selectivity for rare earth elements[38,39], burdensome chemical treatments remain necessary to separate, downstream, the rare earth elements from boron.

A promising yet unexplored pretreatment to support physical separation of individual rare earth elements is selective sulfidation, due to the well-known differences in physical properties between oxide and sulfide phases. Oxides and sulfides are readily separated using economical and environmentally benign physical methods, such as magnetic separation and froth flotation. Sulfidation has previously been applied for numerous transition metal separations from mixed compounds or solid solutions. Examples encompass iron-nickel from laterite[40], nickel-manganese-cobalt-lithium from battery cathodes[41], and zinc-iron-silicon from lead smelter slag[42,43]. Furthermore, sulfidation chemistry utilizes proven reactor technologies[44], and is conducted in industrial settings for nickel extraction[45]. Nevertheless, despite encouraging results for other system chemistries, selective sulfidation has previously never been attempted for rare earth element processing. Herein, we present a thermodynamic framework for the selective sulfidation of individual rare earth oxides, oxysulfides, and sulfides to enable physical separation of individual rare earth elements. We consider the presence of transition metal impurities such as iron, and explore the role of carbon as a process lever to control sulfidation selectivity. For the first time, we then experimentally demonstrate selective sulfidation and desulfidation in the iron-scandium oxide, iron-lanthanum sulfide, and praseodymium-neodymium-dysprosium oxide systems, as a potential pretreatment for isolation of individual rare earth elements via physical separation methods.

Methods

Thermodynamic Framework

While the most commercially relevant rare earth element (RE) minerals are the fluorocarbonate bastnaesite and the phosphates monazite and xenotime, the mixed anion thermodynamics of RE-C-O-F-S and RE-P-O-S systems are thus far unexplored, but presumably different. The rare earth sesquioxide is chosen as a mineral agnostic system for thermodynamic and experimental study of selective sulfidation for rare earth elements. Numerous technologies exist to convert fluorocarbonates and phosphates to oxides without complete hydrometallurgical dissolution[2,15,16,46]. Pyrometallurgical sulfidation of a rare earth sesquioxide (Ln_2O_3) with gaseous, diatomic elemental sulfur (S_2) to form sulfur dioxide and a rare earth sesquisulfide (Ln_2S_3) via a rare earth oxysulfide intermediate (Ln_2O_2S) may be described by the following reactions:



Equation 1 may be rebalanced for the oxides of cerium and praseodymium, which are more stable with metal valencies of +4 and +3,+4 respectively. While hydrogen sulfide and carbon disulfide have classically been employed for sulfidation of rare earth oxides[47], elemental sulfur is employed in this study due to fact that those reagents have previously been shown to be non-selective in sulfidation[48]. The predominant allotrope of sulfur above 800 °C is a diatomic gas[49]. Sulfidation of a transition metal impurity, here iron oxide, is described by a similar reaction.



In Equation 3, the magnetite stoichiometry of iron oxide is considered, as it is the last stable oxide of iron before sulfidation occurs[50]. At equilibrium, the diatomic sulfur and sulfur dioxide partial pressures (P_{S_2} and P_{SO_2} respectively) required for Equations 1-3 to be thermodynamically spontaneous may be related to the standard Gibbs energy of reaction ($\Delta_r G^\circ$) gas constant (R), absolute temperature (T), and activities of condensed metal compound reactants and products (a).

$$\frac{P_{S_2}^2}{P_{SO_2}^3} = \frac{e^{\frac{\Delta_r G^\circ}{RT}} a_{Ln_2O_2S_3}^{\frac{4}{3}}}{a_{Ln_2O_3}^4} \quad (4)$$

$$\frac{P_{S_2}^2}{P_{SO_2}^3} = \frac{e^{\frac{\Delta_r G^\circ}{RT}} a_{Ln_2S_3}^{\frac{2}{3}}}{a_{Ln_2O_2S_3}^{\frac{2}{3}}} \quad (5)$$

$$\frac{P_{S_2}^{\frac{4}{5}}}{P_{SO_2}^{\frac{6}{5}}} = \frac{e^{\frac{\Delta_r G^\circ}{RT}} a_{FeS}^{\frac{6}{5}}}{a_{Fe_3O_4}^{\frac{2}{5}}} \quad (6)$$

Assuming the metal compound reactants and products are non-volatile, and that the gas phase only contains sulfur-oxygen species at a given temperature and pressure, the Gibbs phase rule indicates the equilibrium sulfur dioxide partial pressure is a direct function of diatomic sulfur partial pressure. Isobars depicting equilibrium sulfur dioxide partial pressure as a function of diatomic sulfur partial pressure at a total pressure of 1 atmosphere for temperatures of 800 °C, 1000 °C, 1200 °C, and 1400 °C can be calculated, here using FactSage 8.0 with the FactPS database. From these isobars, a stoichiometric-independent ratio of the partial pressure of diatomic sulfur to sulfur dioxide may be defined and related to the stoichiometrically-dependent sulfur to sulfur dioxide ratios in Equations 4-6. The sulfur to sulfur dioxide ratio required to sulfidize an oxide or oxysulfide, or similarly “desulfidize” a sulfide or oxysulfide, may be defined based on the stoichiometrically dependent ratios of the activities. Selective sulfidation of rare earth or transition metal elements from a mixed metal compound feedstock promotes the formation of sulfide phases that are naturally immiscible with oxide and oxysulfide feedstock phases. Similarly, oxide and oxysulfide phases may be precipitated from mixed sulfide feeds via selective desulfidation of target elements. Elements partitioned into different phases may thereby be liberated and physically separated from one another using technologies such as magnetic separation or froth flotation, providing an opportunity to replace expensive, energy-intensive hydrometallurgical separation with cleaner, cheaper, physical separations. In Figure 1, we compare the diatomic sulfur to sulfur dioxide partial pressure ratios to sulfidize various mineral phases of interest; iron oxide, scandium oxysulfide, and lanthanum oxysulfide. Temperatures of 800 °C, 1000 °C, and 1200 °C are considered, and the partial pressure ratio is presented as a function of metal compound activity ratios, calculated using FactSage 8.0 with the FactPS database supplemented with literature data[51]. Due to the differences in sulfidation reaction stoichiometry between iron oxide and rare earth oxysulfides, a stoichiometric independent activity ratio of product (A_{M-S}) to reactant (A_{M-O-S}) is employed, illustrated here for Equation 5:

$$\frac{A_{M-S}}{A_{M-O-S}} = \frac{a_{Ln_2S_3}^{\frac{2}{3}}}{a_{Ln_2O_2S_3}^{\frac{2}{3}}} \quad (7)$$

A similar relation may be defined for Equation 6. At an activity ratio of 1, the diatomic sulfur to sulfur dioxide partial pressure ratio for sulfidation or desulfidation is equivalent to that determined for pure, immiscible reactants and products as found in a Kellogg[52] or Pourbaix[53] diagram. This sulfur to sulfur dioxide partial pressure ratio is defined as the *pure-phase sulfur to sulfur dioxide ratio*. As shown in Figure 1, formation of a sulfide from iron oxide necessitates lower diatomic sulfur to sulfur dioxide partial pressure ratios than from a rare earth oxysulfides at a given ratio of reactant and product activities. This is consistent with Goldschmidt geochemical classification[54] of elements, where iron is observed to be more chalcophilic than the highly lithophilic rare earth elements. In Figure 2, we compare the diatomic sulfur to sulfur dioxide partial pressure ratios to sulfidize rare earth oxysulfides at 1400 °C as a function of metal compound activity ratios, calculated using FactSage 8.0 with the

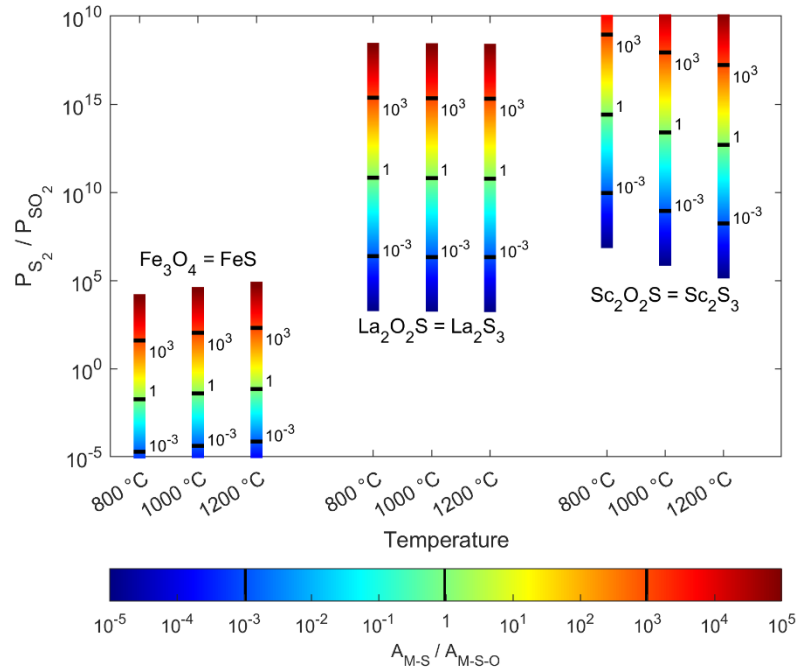
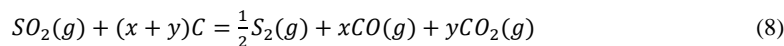


Figure 1: Sulfidation series for iron and rare earth oxides. The sulfur to sulfide dioxide partial pressure ratio at a product and reactant activity ratio of unity is defined as the *pure-phase sulfur to sulfur dioxide ratio*, corresponding to the gas ratio required for sulfidation, as reported in a Kellogg[52] or Pourbaix[53] diagram. (Color images available online).

FactPS database supplemented with literature data[51,55]. The series in which individual rare earth oxysulfides form sulfides with increasing diatomic sulfur to sulfur dioxide partial pressure ratios is highly dependent on the oxysulfide and sulfide activities in the system. Presently, solution thermodynamics of mixed RE-O-S systems are not well-established, yet documented mixed metal oxide and sulfide compound formation[56–59] suggests mixing behavior with large deviations from ideality that are difficult to accurately capture through predictive computational methods[60].

Thermodynamically-spontaneous sulfidation of rare earth oxysulfides at 1400 °C with a reactant and product activity ratio of unity requires a diatomic sulfur to sulfur dioxide partial pressure ratio on the order of $10^{10} - 10^{12}$. This suggests that conversion of rare earth oxysulfide to sulfide will be thermodynamically limited by accumulation of sulfur dioxide within the reactor. One option to minimize sulfur dioxide accumulation in a sulfidation reactor is to carbothermally reduce sulfur dioxide in situ back into diatomic sulfur gas, forming a *carbothermally-driven sulfur reflux* within a sulfidation reactor:



The reducing power of carbon for sulfur dioxide, effectivity the carbon monoxide to carbon dioxide ratio (x/y in Equation 8), is in turn described by the Boudouard equilibrium. Equations 4-6 show that the selectivity of sulfidation is therefore determined from the thermodynamic activities of the reactant and product compounds, as well as possibly by the diatomic sulfur to sulfur dioxide partial pressure ratio. The later can be modulated via the extent of the carbothermally-driven sulfur reflux. Since the mixing thermodynamics of mixed RE-O-S systems are not well-understood, and will likely vary based on fluctuations in composition between mineral feedstocks and ore bodies, we herein explore the role of the diatomic sulfur to sulfur dioxide partial on sulfidation and desulfidation selectivity independent of mineral solution thermodynamics. In the following sections, we experimentally demonstrate selective sulfidation and desulfidation in the absence of carbon for mixed iron and rare earth compounds. We then explore the role of carbon content on sulfide product formation and selectivity in mixed rare earth oxides.

Experimental Framework

Sulfidation and desulfidation experiments were conducted in an aluminum oxide packed bed reactor at temperatures ranging from 800 °C to 1400 °C, following previously described designs and methodology[41]. The sulfidizing agent was vaporized elemental sulfur (S_x , 99.5% purity, Acros Organics). Argon (Ar, 99.95%, UHP300, Airgas) was used as a carrier gas for vaporized sulfur, with sulfur partial pressure monitored by calibrating evaporation rate to an H_2S tracer. For desulfidation experiments, volatilized sulfur was combusted upstream of the reactor with oxygen (O_2 , 99.95%, UHP300, Airgas) to produce sulfur dioxide to be used in conjunction with argon as carrier gas.

For demonstration of selective sulfidation with mixed pure oxides, iron(III) oxide (Fe_2O_3 , 99.85% metals basis, Alfa Aesar), scandium(III) oxide (Sc_2O_3), neodymium(III) oxide (Nd_2O_3 , 99.9%-Nd REO basis, Strem Chemicals), praseodymium (III,IV) oxide (Pr_6O_{11} , 99.9%-Pr REO basis, Strem Chemicals) and dysprosium(III) oxide (Dy_2O_3 , 99.9% Dy, REO basis, Strem Chemicals) were utilized as oxide precursors. When selective sulfidation was conducted in the presence of carbon, activated carbon (C, Alfa Aesar, 20 μm) was utilized. For demonstration of selective desulfidation of mixed pure sulfides, iron sulfide (FeS , 99.95%, Alfa Aesar) and lanthanum sulfide (La_2S_3 , 99.5% metals basis purity, Strem Chemical) were utilized as precursors.

Selective sulfidation / desulfidation campaigns at temperatures ranging from 800 °C to 1400 °C were conducted at scales ranging from 2-3 grams of feed material. While not strictly representative of natural abundances, equal molar or mass ratios of oxides are utilized so that trends in product purity and impurity solubility are readily apparent for different sulfidation conditions. Heating and cooling rates of 5 °C / minute were utilized. Reaction times were 50 minutes, with a 5 minute hold at temperature before and after sulfidation / desulfidation. Argon carrier gas flowrates were determined so that the gas residence time through the packed bed was on the order of 0.1 seconds. The compositions of product gasses were analyzed for oxygen, carbon monoxide, carbon dioxide, sulfur dioxide, and hydrogen sulfide content via an infrared /electrochemical gas analyzer (IR208, Infrared

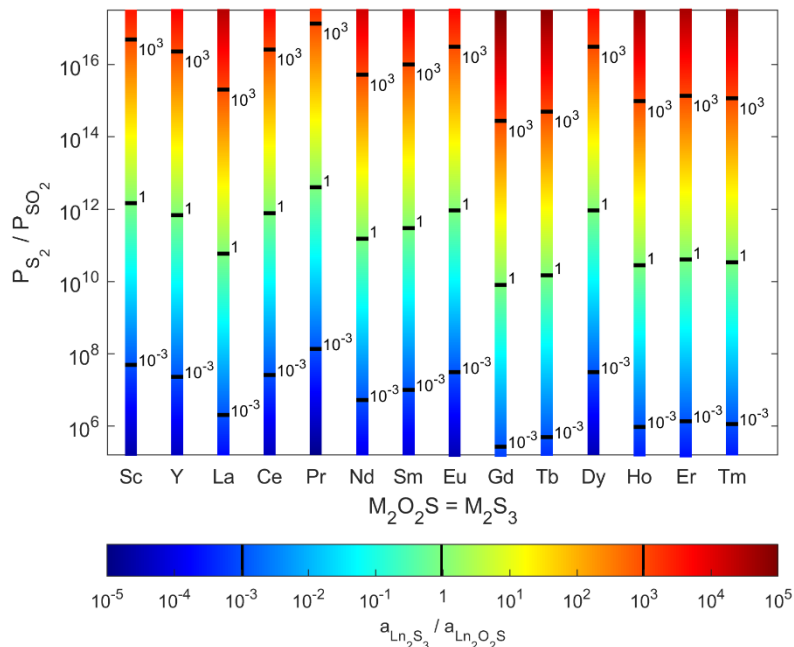


Figure 2: Sulfidation series for rare earth oxysulfides. The sulfur to sulfide dioxide partial pressure ratio at a product and reactant activity ratio of unity is defined as the *pure-phase sulfur to sulfur dioxide ratio*, corresponding to the gas ratio required for sulfidation, as reported in a Kellogg[52] or Pourbaix[53] diagram. (Color images available online).

Industries). The compositions of sulfidation / desulfidation products were analyzed via SEM/EDS (SEM: JEOL JSM-6610LV, JEOL Ltd., EDS: Sirius SD detector, SGX Sensortech Ltd.) and QXRD (Panalytical X'Pert MPD diffractometer).

Selective sulfidation of iron from mixed iron and scandium oxides at a 1:1 mass ratio was conducted at temperatures of 800 °C and 1000 °C. Oxide precursors were ground to a particle size of sub-44 microns and loaded into the reactor bed at a porosity of approximately 80%. Sulfur gas was supplied at a partial pressure on the order of 0.1 atm. The sulfidation reaction occurred at such a rate that the sulfur to sulfur dioxide molar ratio within the reactor was approximately 10:1. From Figure 1, under such conditions iron was thermodynamically predicted to form a sulfide, whereas scandium was predicted to be stable as an oxysulfide.

Selective sulfidation was also conducted for a multielement lanthanide system of equimolar mixed praseodymium oxide, neodymium oxide, and dysprosium oxide. Sulfidation was conducted at a temperature of 1400 °C with and without the addition of carbon, with oxide particle sizes on the order of 10 microns and bed porosities on the order of 80%. Sulfur gas was supplied at a partial pressure of approximately 0.05 atm to 0.2 atm. In the absence of carbon, the sulfidation reaction occurred at such a rate that the sulfur to sulfur dioxide molar ratio within the reactor was approximately 10:1. For sulfidation in the presence of carbon, activated carbon was mixed in with the oxide charge at carbon to oxide molar ratios of 1.25:1, 2.5:1, 3.75:1, and 6:1. From Figure 2, by varying the carbon addition and therefore the sulfur to sulfur dioxide molar ratio, oxysulfide and sulfides of rare earth elements are predicted to form.

Selective desulfidation for mixed iron and lanthanum sulfides at a 1:1 mass ratio was demonstrated at a temperature of 1000 °C. Sulfide powders were loaded into the reactor bed at a porosity of approximately 80%. Sulfur and sulfur dioxide gasses were introduced to the reactor at mole ratios varying from 10:1 to 1:10 over the course of the experiment, constituting a total partial pressure of between 0.05 atm and 0.2 atm in the argon carrier gas. From Figure 1, under such conditions iron was thermodynamically predicted to remain stable as a sulfide, whereas lanthanum sulfide was predicted to desulfidize to form an oxysulfide. The results of selective sulfidation and desulfidation trials are presented in the following section.

Results and Discussion

Selective Sulfidation of Iron-Scandium Oxides

An equimolar mixture of scandium and iron oxides (46 wt% and 54 wt% respectively) was selectively sulfidized as a potential pretreatment to facilitate physical separation of iron and scandium, following the methodology described above. Sulfidation products were analyzed via QXRD. Following sulfidation, the only remaining crystalline compound of iron was iron sulfide, making up 28 wt% and 29 wt% after selective sulfidation at 800 °C and 1000 °C respectively. Meanwhile, the only crystalline phase of scandium observed after sulfidation was scandium oxide, decreasing in composition from 38 wt% to 30 wt% as sulfidation temperature rose from 800 °C to 1000 °C. The preferential partitioning of scandium and iron to separate oxide and sulfide phases respectively suggests that selective sulfidation is a promising pretreatment to facilitate physical separation of scandium and iron. At the higher sulfidation temperature, the amorphous content correspondingly increased from 33 wt% to 42 wt%. As shown in Figure 1, thermodynamically scandium oxide sulfidation to oxysulfide is expected to accompany iron sulfide formation. The presence of crystalline scandium oxide following the sulfidation treatment suggests that the sulfidation of scandium oxide to oxysulfide is kinetically sluggish compared to sulfidation of iron oxide.

Figure 3 illustrates the distribution of oxygen, sulfur, iron, and scandium following sulfidation at 1000 °C, as measured via EDS element mapping. Scandium is revealed to partition into oxygen-rich phases, whereas iron is observed to partition into sulfur-rich phases, confirming the results of QXRD analysis. Under the sulfidation conditions of the experiment, scandium oxide phases are observed to exhibit sulfur and iron solubilities of approximately 5 wt% and 15 wt% respectively. Meanwhile, iron sulfide phases exhibit solubilities for oxygen and scandium of approximately 5 wt% to 10 wt% each. Solubilities between scandium oxide and iron sulfide phases are a function of their mixing thermodynamics, defined by the activities of iron and scandium oxide and sulfide compounds in the system. As shown in Equations 4-6, at thermodynamic equilibrium, ratios of reactant and product activities are set by the sulfur to sulfur dioxide partial pressure ratio in the gas phase.

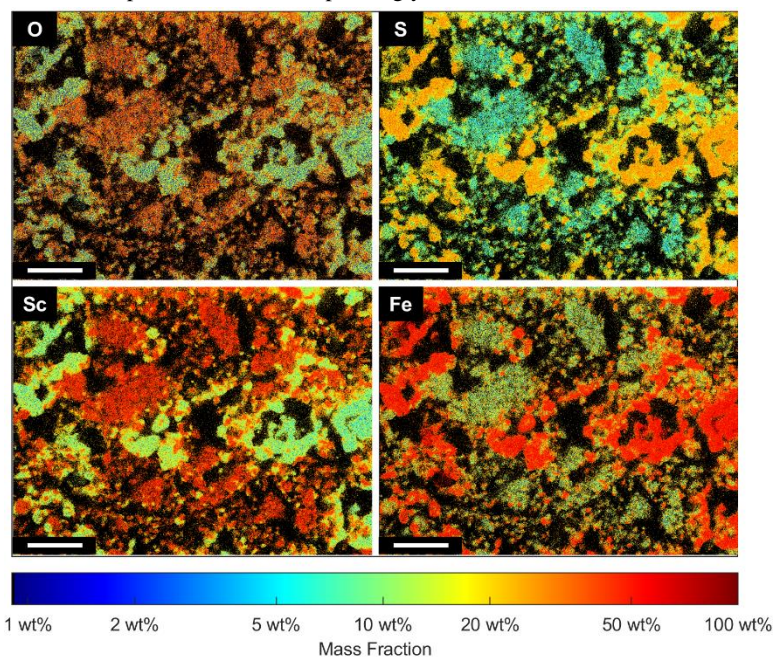


Figure 3: EDS map detailing distribution of O, S, Sc, and Fe following selective sulfidation of mixed iron-scandium oxides. Following selective sulfidation, iron was observed to partition into a sulfide phase, while scandium remained as an oxide. Scale bars correspond to 50 μm. (Color images available online).

Therefore, the solubility between scandium oxide and iron sulfide products are controlled by the composition of the sulfidation atmosphere. As shown in Figure 1, at increasing temperatures the difference in the *pure-phase sulfur to sulfur dioxide ratio* between sulfidation of iron oxide and scandium oxysulfide falls, corresponding to a decrease in sulfidation selectivity and increase in solubility between oxide and sulfide products. This predicted drop in selectivity likely corresponds to the decrease in crystalline scandium oxide content and increase in multi-metal amorphous compounds at increasing sulfidation temperature. Further thermodynamic analysis of sulfidation selectivity is hindered by the lack of relevant mixing thermodynamic data for the Sc-Fe-O-S system. Similarly, limited knowledge of the thermal activation of scandium oxide sulfidation kinetics leads to difficulties in distinguishing the roles of thermodynamics and kinetics in selective sulfidation for iron-scandium separation.

Selective Sulfidation of Mixed Lanthanide Oxides

For selective sulfidation of mixed lanthanide (Ln) oxides as a pretreatment to facilitate their physical separation, an equimolar mixture of praseodymium, neodymium, and dysprosium oxides was used as a feedstock. Carbon content was varied as a means to control the sulfur to sulfur dioxide partial pressure ratio in the gas atmosphere. The conversions at 1400 °C of equimolar mixed praseodymium, neodymium, and dysprosium oxides to oxysulfide and sulfide products, and amorphous carbon to carbon monoxide, are depicted in Figure 4 as functions of carbon content and supplied sulfur gas partial pressure. While challenges remain in consistently controlling the sulfur partial pressure at the scale of this experiment, the fractional molar conversion of oxide sulfidation is shown to generally increase with increasing carbon feed content. This confirms the role of the *carbothermally driven sulfur reflux* (Equation 8) in increasing the sulfur to sulfur dioxide molar gas ratio. Surprisingly, the conversion of carbon-free sulfidation of the mixed rare earth oxides is observed to be 50% higher than with an oxide to carbon molar feed ratio of 1.25. Further research into Ln-O-S-C thermodynamics are likely needed to understand the origin of this behavior. The fractional molar conversion of carbon to carbon monoxide meanwhile showed a slight increase with carbon content, generally remaining on the order of 30% to 35%. Whether this conversion was limited due to the formation of byproduct carbon-sulfur gasses[61], or intrinsic to the thermodynamics and kinetics of the *carbothermally-driven sulfur reflux*, remains to be determined. Carbon dioxide was not detected to form at these temperatures in measurable quantities due to the Boudouard equilibrium. Under the reaction and mass transport conditions of these experiments, the sulfidation rate of the mixed rare earth oxide was observed to vary to the first order with sulfur partial pressure, independent of carbon content, until the maximum conversion was reached. However, detailed analysis of internal and external mass transport limitations[62–64] would be required to rigorously relate sulfidation kinetics observed in this experiment to the intrinsic chemical kinetics of rare earth oxide sulfidation reactions.

Sulfidized product phases as a function of carbon content are identified via XQRD and depicted in Table 1. With increasing carbon feed content, the total amorphous oxysulfide content of the sulfidized product increases. At a carbon to rare earth oxide molar feed ratio of 1.25, the crystalline content of Ln₂O₂S oxysulfide phases is approximately the same as for carbon-free sulfidation, despite carbon-free sulfidation exhibiting a 50% higher sulfidation conversion. At a carbon to rare earth oxide molar feed ratio of 2.5, a more sulfur-rich Ln₁₀OS₁₄ oxysulfide is detected. At carbon to rare earth oxide feed ratios of 3.75 and 6, the crystalline products are observed to be sulfides, with the sulfur content of the crystalline compound increasing with carbon feed content. XQRD suggests that the first sulfide to form is that

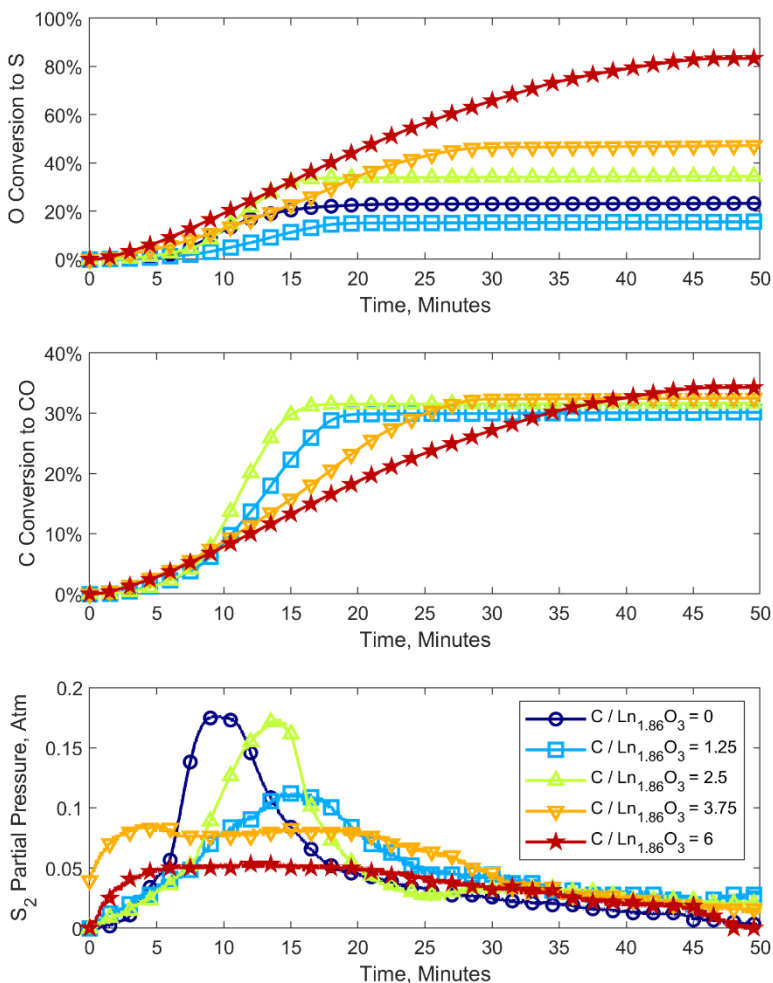


Figure 4: Conversion of oxide to sulfide and carbon to carbon monoxide as functions of carbon content and sulfur gas partial pressure during selective sulfidation of mixed praseodymium-neodymium-dysprosium oxides. Increasing carbon content in the feed leads to higher conversion of oxides to sulfides by increasing the sulfur to sulfur dioxide partial pressure ratio, demonstrating the *carbothermally-driven sulfur reflux* (Equation 8). (Color images available online).

of neodymium, consistent with *pure-phase sulfur to sulfur dioxide ratios* presented in Figure 2. The selective partitioning of neodymium to a sulfide phase from mixed, amorphous lanthanide oxysulfide suggests that selective sulfidation is a promising pretreatment to promote physical separation of individual rare earth elements. Due to the similar size and electronic structure of lanthanides, atomic substitution between rare earth elements in the crystalline sulfide product and amorphous oxysulfide phases is likely to occur. Further analysis via advanced micrographic techniques, such as WDS/EPMA, is necessary to determine the spatial distributions and purities of product phases. Presently, the lack of lanthanide thermodynamic compound data for $\text{Ln}_{10}\text{OS}_{14}$, Ln_3S_4 , and LnS_2 , complicates thermodynamic predictions of sulfidation selectivity, as these compounds are presently excluded from the sulfidation series in Figures 1 and 2. Furthermore, the absence of mixing thermodynamic data for Ln-O-S systems presently negates the ability to inform solubility and product purity through activity models. Nevertheless, *carbothermally driven sulfur reflux* is an attractive avenue to control of the sulfur to sulfur dioxide partial pressure ratio to maximize sulfidation selectivity, subject to the solution thermodynamics of rare earth feedstock compounds and sulfidation products.

Selective Desulfidation of Iron-Lanthanum Sulfide

Due to differences in oxide and sulfide solution behavior, some separation challenges may be easier to overcome starting from a mixed sulfide instead of a mixed oxide. Under such a scenario, the thermodynamic framework presented herein can simultaneously be employed to describe a selective desulfidation process. Reversing Equations 1 and 2, the oxygen source for desulfidation is sulfur dioxide, with desulfidation potential still controlled by a sulfur to sulfur dioxide molar gas ratio. Selective desulfidation of iron from a 1:1 mass ratio mixture of iron and lanthanum sulfides (FeS and La_2S_3) was conducted herein at a temperature of 1000 °C, with sulfur to sulfur dioxide partial pressure ratios ranging from 10:1 to 1:10. In Figure 5, SEM/EDS element maps depict the spatial distribution of oxygen, sulfur, lanthanum, and iron in the selectively desulfidized product. Iron was found to remain stable in sulfide phases, as predicted from Figure 1 for the conditions of the experiment. Meanwhile, lanthanum was found to selectively desulfidize under these conditions as predicted from Figure 1, partitioning preferentially into oxysulfide phases with stoichiometries of approximately $\text{La}_2\text{O}_2\text{S}$ and $\text{La}_{10}\text{OS}_{14}$. The observed solubility of iron in the $\text{La}_2\text{O}_2\text{S}$ and $\text{La}_{10}\text{OS}_{14}$ product phases was approximately 2 at% and 10 at% respectively, whereas the solubilities of lanthanum and oxygen in the iron sulfide phases were approximately 1 at% to 2 at% each. As shown in Figure 1 and Equations 4-6, decreasing the sulfur to sulfur dioxide partial pressure ratio would work to decrease the activity of iron sulfide and increase the activity of iron oxide. An optimum sulfur to sulfur dioxide partial pressure ratio therefore exists to minimize the solubility of iron in lanthanum rich phases and lanthanum in iron rich phases. While determination of the optimal sulfur to sulfur dioxide partial pressure ratio is mired by a lack of La-Fe-O-S solution data, these results suggest that selective desulfidation is a feasible pretreatment to accomplish challenging materials separations via physical methods.

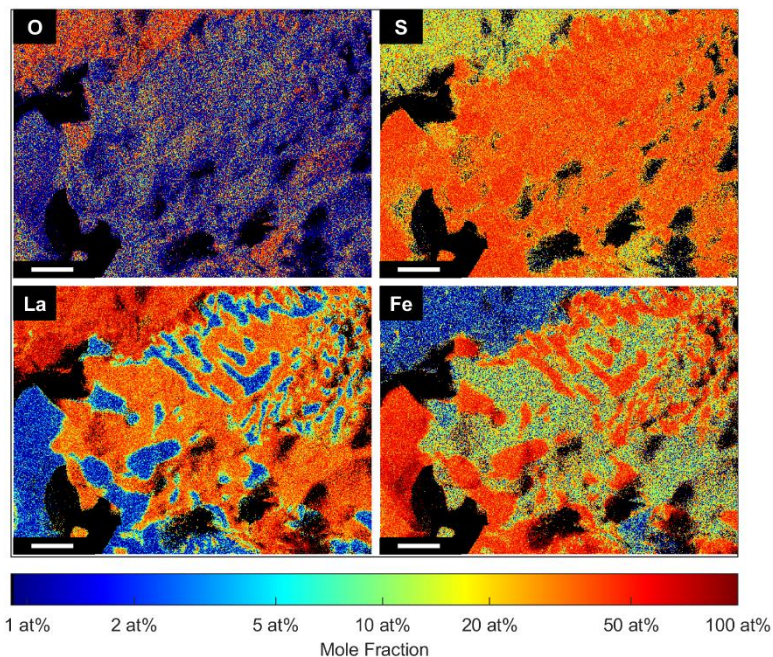


Figure 5: EDS map detailing distribution of O, S, La, and Fe following selective desulfidation of mixed iron-lanthanum sulfides. Following selective desulfidation, lanthanum was observed to partition into oxysulfide phases, while iron remained as a sulfide. Scale bars correspond to 15 μm . (Color images available online).

Table 1: QXRD analysis of praseodymium-neodymium-dysprosium oxide (REO) sulfidation products.

QXRD wt %	C/REO = 0	C/REO = 1.25	C/REO = 2.5	C/REO = 3.75	C/REO = 6
Pr_2O_3	-	1%	-	-	-
$\text{Nd}_2\text{O}_2\text{S}$	17%	12%	-	-	-
$\text{Nd}_{10}\text{OS}_{14}$	-	-	25%	-	-
$\text{Dy}_2\text{O}_2\text{S}$	27%	28%	12%	-	-
$\text{Pr}_2\text{O}_2\text{S}$	3%	1%	-	-	-
Nd_3S_4	-	-	-	9%	-
Nd_2S_3	-	-	-	16%	16%
NdS_2	-	-	-	-	1%
Amorphous	53%	58%	63%	75%	83%

Summary

In this study, mixed oxides were used as feedstocks for selective sulfidation / desulfidation in order to provide minerals-agnostic test cases. In practice, rare earth minerals most commonly occur as fluorocarbonates or phosphates, with rare earth elements contained at grades that may differ by orders of magnitude between one element and the next. While a variety of methods exist to convert fluorocarbonates and phosphates to oxides, understanding the sulfidation behavior of oxyhalides and phosphates will be necessary to design a rare earth physical separation process from mineral feedstocks. Equal molar or mass ratios of oxides were employed in this study so that metallic elements were at sufficient concentrations to readily observe trends in product purity and impurity solubility with different sulfidation conditions. Solution thermodynamics, if available, may be used to predict sulfidation behavior as shown herein even for feedstocks of very different grades. However, knowledge of solution thermodynamics will have to be developed for the minerals chemistries relevant to a given separation process. For design of physical separation processes for elements following selective sulfidation or desulfidation, an understanding of product phase nucleation, growth, and liberation phenomenon will be necessary. Fortunately, liberation and physical separation of sulfides from oxides remains a vibrant area of research due to the growing need to adapt existing mineral beneficiation processes to declining ore grades[65,66].

Overall, our preliminary results suggest that selective sulfidation and selective desulfidation are promising new avenues to promote physical separation of individual rare earth elements (RE) and their impurities. We present a thermodynamic framework for modelling selectivity in sulfidation and desulfidation processes that proves viable to predict overall trends in sulfidation behavior and selectivity. However, predicting product phase purities and impurity solubilities is hindered by an absence of mixing thermodynamics and activity models for RE-O-S solutions and their impurities. We identify the ratio of sulfur to sulfur dioxide partial pressures as a key process lever for selective sulfidation, which we show may be modulated through the use of carbon additions in the system. Yet, knowledge of sulfidation kinetics for rare earth compounds will need to be developed in order to balance the rate of sulfur dioxide production and its rate of carbothermic reduction in achieving a target sulfur to sulfur dioxide partial pressure ratio in the reactor. We successfully demonstrate proof-of-concept selective sulfidation and desulfidation for iron-scandium, iron-lanthanum, and lanthanide-lanthanide separations. These results illuminate a path forward for competitive rare earth separation, where physical separations become a new possibility, alleviating the need for complete hydrometallurgical dissolution and multi-stage liquid-liquid solvent extraction.

Acknowledgements

The authors wish to thank Dr. Hirotaka Higuchi for providing samples of scandium oxide. Part of this work was funded from the DOE-AMO-EERE Office under project DE-EE0008316.

References

1. T. Cheisson and E. J. Schelter, *Science* (80-.), **363**, 489 (2019).
2. B. Zhao, J. Zhang, and B. Schreiner, *Separation Hydrometallurgy of Rare Earth Elements* (Springer International Publishing AG Switzerland, 2016).
3. In *CRC Handb. Chem. Phys.*, 97th Editi (2016), pp. 14–17.
4. U.S. Geological Survey, *Mineral Commodity Summaries 2021* (2021).
5. U.S. Department of Energy, *Critical Minerals and Materials* (2020).
6. K. Binnemans, P. T. Jones, T. Müller, and L. Yurramendi, *J. Sustain. Metall.* **4**, 126 (2018).
7. S. M. Jowitz, T. T. Werner, Z. Weng, and G. M. Mudd, *Curr. Opin. Green Sustain. Chem.* **13**, 1 (2018).
8. G. Bailey, P. J. Joyce, D. Schrijvers, R. Schulze, A. M. Sylvestre, B. Sprecher, E. Vahidi, W. Dewulf, and K. Van Acker, *Resour. Conserv. Recycl.* **155**, 104675 (2020).
9. J. Kim and G. Azimi, *Hydrometallurgy* **191**, (2020).
10. W. Wang, Y. Pranolo, and C. Y. Cheng, *Hydrometallurgy* **108**, 100 (2011).
11. J. Anawati, R. Yuan, J. Kim, and G. Azimi, in *Miner. Met. Mater. Ser.* (Springer, 2020), pp. 77–90.
12. R. P. Narayanan, N. K. Kazantzis, and M. H. Emmert, *ACS Sustain. Chem. Eng.* **6**, 1478 (2018).
13. C. R. Borra, J. Mermans, B. Blanpain, Y. Pontikes, K. Binnemans, and T. Van Gerven, *Miner. Eng.* **92**, 151 (2016).
14. F. Meng, X. Li, L. Shi, Y. Li, F. Gao, and Y. Wei, *Miner. Eng.* **157**, (2020).
15. A. Jordens, Y. P. Cheng, and K. E. Waters, *Miner. Eng.* **41**, 97 (2013).
16. A. Kumari, R. Panda, M. K. Jha, J. R. Kumar, and J. Y. Lee, *Miner. Eng.* **79**, 102 (2015).
17. H. Vogel and B. Friedrich, in *Light Met. 2018* (Springer Berlin Heidelberg, Berlin, Heidelberg, 2018), pp. 1507–1517.
18. J. C. K Lee and Z. Wen, *Nat. Sustain.* **1**, 598 (2018).
19. E. Vahidi and F. Zhao, *J. Environ. Manage.* **203**, 255 (2017).
20. L. C. O. N. Hall and S. Kelley, *Yangibana Project* (2015).
21. T. Ciuculescu, B. Foo, R. Gowans, K. Hawton, C. Jacobs, and J. Spooner, *Nechalacho Rare Earth Elements Project* (2013).
22. N. M. Limited, *Browns Range Project* (2014).
23. P. R. Limited, *Q. Rep.* (2012).
24. X. Z. Li, L. P. Zhou, L. L. Yan, Y. M. Dong, Z. L. Bai, X. Q. Sun, J. Diwu, S. Wang, J. C. Bünzli, and Q. F. Sun, *Nat. Commun.* **9**, (2018).
25. R. F. Higgins, T. Cheisson, B. E. Cole, B. C. Manor, P. J. Carroll, and E. J. Schelter, *Angew. Chemie Int. Ed.* **59**, 1851 (2020).

26. T. Norgate and S. Jahanshahi, *Miner. Eng.* **23**, 65 (2010).
27. B. J. Skinner, *Sci. Am.* **64**, 258 (1976).
28. B. J. Skinner, *Proc. Natl. Acad. Sci. USA* **76**, 4212 (1979).
29. K. Murase, K. Shinozaki, Y. Hirashima, K. ichi Machida, and G. ya Adachi, *J. Alloys Compd.* **198**, 31 (1993).
30. T. Uda, K. T. Jacob, and M. Hirasawa, *Science (80-)*. **289**, 2326 (2000).
31. J. C. Elgin, *Light Met.* 2019 1395 (2019).
32. J. Andrade-Gamboa, J. Andrade-Gamboa, and D. M. Pasquevich, *Metall. Mater. Trans. B Process Metall. Mater. Process. Sci.* **31**, 1439 (2000).
33. B. Onghena, C. R. Borra, T. Van Gerven, and K. Binnemans, *Sep. Purif. Technol.* **176**, 208 (2017).
34. J. Wang and H. Hu, *Miner. Eng.* **160**, 106711 (2021).
35. C. R. Borra, J. Mermans, B. Blanpain, Y. Pontikes, K. Binnemans, and T. Van Gerven, *Miner. Eng.* **92**, 151 (2016).
36. R. P. Narayanan, N. K. Kazantzis, and M. H. Emmert, *ACS Sustain. Chem. Eng.* **6**, 1478 (2018).
37. J. Anawati, R. Yuan, J. Kim, and G. Azimi, *Selective Recovery of Scandium from Nickel Laterite Ore by Acid Roasting–Water Leaching* (Springer International Publishing, 2020).
38. X. Yin, Y. Wang, X. Bai, Y. Wang, L. Chen, C. Xiao, J. Diwu, S. Du, Z. Chai, T. E. Albrecht-Schmitt, and S. Wang, *Nat. Commun.* **8**, (2017).
39. M. Firdaus, M. A. Rhamdhani, Y. Durandet, W. J. Rankin, and K. McGregor, *J. Sustain. Metall.* **2**, 276 (2016).
40. C. T. Harris, J. G. Peacey, and C. A. Pickles, *Miner. Eng.* **54**, 21 (2013).
41. C. Stinn and A. Allanore, in *Ni-Co 2021 5th Int. Symp. Nickel Cobalt*, edited by C. Anderson, G. Goodall, S. Gostu, D. Gregurek, M. Lundström, C. Meskers, S. Nicol, S. Peuraniemi, F. Tesfaye, P. K. Tripathy, S. Wang, and Y. Zhang (Springer Nature Switzerland AG, 2021), pp. 99–110.
42. J. Han, W. Liu, D. Wang, F. Jiao, and W. Qin, *Metall. Mater. Trans. B Process Metall. Mater. Process. Sci.* **47**, 344 (2016).
43. J. Han, W. Liu, D. Wang, F. Jiao, and W. Qin, *Metall. Mater. Trans. B* **47**, 344 (2015).
44. K. Adham and C. Lee, in *Toward Clean Metall. Process. Profit, Soc. Environ. Steward.* (2012), pp. 109–116.
45. F. K. Crundwell, M. S. Moats, V. Ramachandran, T. G. Robinson, and W. G. Davenport, *Extractive Metallurgy of Nickel, Cobalt, and Platinum-Group Metals* (Elsevier, 2011).
46. R. R. Merritt, *J. Less-Common Met.* **166**, 211 (1990).
47. T. Kaneko, Y. Yashima, E. Ahmadi, S. Natsui, and R. O. Suzuki, *J. Solid State Chem.* **285**, 121268 (2020).
48. P. Afanasiev, L. Fischer, F. Beauchesne, M. Danot, V. Gaborit, and M. Breyse, *Catal. Letters* **64**, 59 (2000).
49. B. Meyer, *Chem. Rev.* **76**, 367 (1976).
50. N. Chakraborti, *Can. J. Chem. Eng.* **61**, 763 (1983).
51. R. K. Dwivedi and D. A. R. Kay, *Metall. Trans. B* **15**, 523 (1984).
52. H. H. Kellogg, *Trans. Metall. Soc. AIME* **230**, 1622 (1964).
53. M. J. N. Pourbaix and M. C. M. Rorive-Bouté, *Discuss. Faraday Soc.* **4**, 139 (1948).
54. V. M. Goldschmidt, *J. Chem. Soc.* 655 (1937).
55. A. I. Kriklya, A. S. Bolgar, and N. Y. Pribyl'skii, *Sov. Powder Metall. Met. Ceram.* **31**, 697 (1992).
56. A. K. Kuznetsov, P. A. Tikhonov, M. V. Kravchinskaya, V. M. Iuneev, and L. M. Ivanov, *Dokl. Akad. Nauk SSSR* **231**, 882 (1976).
57. P. A. Tichonov, I. Proks, and L. Kosa, *Silikaty* **26**, 165 (1982).
58. I. B. Bakhtiyarov, *Azerbaijanskii Khimicheskii Zhurnal* **4**, (1987).
59. M. M. Asadov and M. M. Abbasov, *Inorg. Mater.* **32**, 280 (1996).
60. M. Chen, B. Hallstedt, and L. J. Gauckler, *Calphad Comput. Coupling Phase Diagrams Thermochem.* **29**, 103 (2005).
61. E. Ahmadi and R. O. Suzuki, *J. Sustain. Metall.* 2021 72 **7**, 437 (2021).
62. H. Y. Sohn and J. Szekely, *Chem. Eng. Sci.* **29**, 630 (1974).
63. H. Y. Sohn and J. Szekely, *Chem. Eng. Sci.* **27**, 763 (1972).
64. H. Y. Sohn and D.-Q. Fan, *Met. Mater. Trans. B* **48B**, 1827 (2017).
65. N. Rötzer and M. Schmidt, *Resources* **7**, 88 (2018).
66. G. Calvo, G. Mudd, A. Valero, and A. Valero, *Resources* **5**, 36 (2016).